161585-0007-F

VARIATIONAL DATA ASSIMILATION FOR NEAR-SHORE WAVES USING THE EXTENDED BOUSSINESQ EQUATIONS

Prepared for: OFFICE OF NAVAL RESEARCH
875 North Randolph Street, Suite 1425
Arlington, Virginia 22203-1995

By: David T. Walker
General Dynamics Advanced Information Systems
1200 Joe Hall Drive
Ypsilanti, MI 48197

Contract Number: N00014-00-D-0114-0007

Date: October 2005

GENERAL DYNAMICS
Advanced Information Systems

REPORT DOCUMENTATION PAGE

Form Approved
OMB No. 0704-0188

1. REPORT DATE *(DD-MM-YYYY)*	2. REPORT TYPE	3. DATES COVERED *(From - To)*
10-31-2005	Final	01 January 2002 - 30 June 2005

4. TITLE AND SUBTITLE
Variational Data Assimilation for Near-Shore Waves Using the Extended Boussinesq Model

5a. CONTRACT NUMBER
N00014-00-D-0114-0007

5b. GRANT NUMBER

5c. PROGRAM ELEMENT NUMBER

6. AUTHOR(S)
David T. Walker
General Dynamics Advanced Information Systems
1200 Joe Hall Drive
Ypsilanti, MI 48197

5d. PROJECT NUMBER

5e. TASK NUMBER

5f. WORK UNIT NUMBER

7. PERFORMING ORGANIZATION NAME(S) AND ADDRESS(ES)
General Dynamics–Advanced Information Systems

8. PERFORMING ORGANIZATION REPORT NUMBER
161585-0007-F

9. SPONSORING/MONITORING AGENCY NAME(S) AND ADDRESS(ES)
Office of Naval Research
875 North Randolph Street, Suite 1425
Arlington, Virginia 22203-1995

10. SPONSOR/MONITOR'S ACRONYM(S)
ONR

11. SPONSORING/MONITORING AGENCY REPORT NUMBER

12. DISTRIBUTION AVAILABILITY STATEMENT
Approved for Public Release: Distribution Unlimited

13. SUPPLEMENTARY NOTES

14. ABSTRACT
This report describes a variational approach for assimilation of single-point, in-situ observations of surface elevation and velocity into the extended Boussinesq model of Wei et al. (1996). The mathematical framework for assimilation is presented, along with applications of the procedure for two cases: monochromatic waves and broad-spectrum irregular waves. Overall the performance of the approach for monochromatic waves is quite good; while for irregular waves, some of the short-wave detail, especially for waves propagating in the along-shore direction, is missed. As part of the development work, an existing parallel Boussinesq model code was improved through addition of run-up, wave-breaking and and bottom-friction models, and a directional wavemaker was implemented.

15. SUBJECT TERMS
Inverse modeling, wave modeling, data assimilation.

16. SECURITY CLASSIFICATION OF:			17. LIMITATION OF ABSTRACT	18. NUMBER OF PAGES	19a. NAME OF RESPONSIBLE PERSON
a. REPORT	b. ABSTRACT	c. THIS PAGE	SAR	29	David T. Walker
U	U	U			19b. TELEPONE NUMBER (*Include area code*) (734)480-5416

Abstract

This report describes a variational approach for assimilation of single-point, in-situ observations of surface elevation and velocity into the extended Boussinesq model of Wei *et al.* (1996). The mathematical framework for assimilation is presented, along with applications of the procedure for two cases: monochromatic waves and broad-spectrum irregular waves. Overall the performance of the approach for monochromatic waves is quite good; while for irregular waves, some of the short-wave detail, especially for waves propagating in the along-shore direction, is missed. As part of the development work, an existing parallel Boussinesq model code was improved through addition of run-up, wave-breaking and and bottom-friction models, and a directional wavemaker was implemented.

Contents

List of Figures

1 Introduction

Coastal regions represent the boundary where the effects of weather systems off-shore impact activities on land. One of the main features of this boundary is the shoaling of waves over the continental shelf. As waves shoal, their amplitude increases, resulting in large loads on near-shore structures, etc. This increase in amplitude can also lead to wave breaking, which can drive near-shore circulation, with the resulting currents playing a significant role in sediment transport and beach erosion. In addition, for amphibious military operations, the near-shore region with its steep and breaking waves, and attendant currents, represents a natural barrier of sorts which needs to be traversed in an efficient fashion. For all of these reasons, there is an abiding interest in the monitoring and prediction of near-shore ocean waves.

This report describes a approach which can be used to take time-histories of velocity and sea-surface elevation from a number of discrete spatial locations and use them to produce a synoptic estimate of the wave field for the region of interest. The approach relies on a variational data assimilation algorithm which makes use of the extended Boussinesq model of Wei *et al.* (1996). In this document, the mathematical framework for assimilation is first presented. It assumes that the Boussinesq model is an exact representation of the physics of near-shore waves, and seeks a solution to the model which best fits the data. The key input to the Boussinesq model which produces the desired solution is the wavemaker source function. To determine the source function which yields the best fit to the data, a cost function, a measure of error in the predictions, is first defined. A set of adjoint equations is then developed. The solution of the adjoint equations is used to calculate the gradient of the cost function with respect to the wave maker source function. This gradient is used in an iterative minimization scheme to determine the source function which yields the minimum error.

In this program, a parallel FORTRAN code was developed that implements the assimilation procedure. As part of the code development, an existing parallel Boussinesq code based on both the formulation and numerical approach of Wei *et al.* (1996), was extended to include modeling for run-up, wave-breaking and bottom friction. In addition both monochromatic and broad-spectrum wavemakers were implemented. This results in a Boussinesq model code capable of generating realistic wave fields either as a product of the assimilation process, or as a direct forward prediction

based on a known incident wave spectrum.

The assimilation procedure was applied to two cases, observations of monochromatic waves and irregular waves. Application of the procedure for monochromatic waves converged quickly and comparison of the estimated time series at the observation locations to the observations shows good agreement between the predictions and observations. Application for irregular waves produces encouraging, but less-accurate results.

In the following sections, the assimilation approach is developed, followed by a description of the Boussinesq model extensions for wave run-up, breaking and bottom friction. Then, simulated data to be used in the assimilation procedure is presented. Application of the procedure to two different situations, monochromatic waves and irregular waves, is then discussed. The conclusions of the study are then presented, along with recommendations for future work.

2 The extended Boussinesq model

The extended Boussinesq model of Wei *et al.* (1996) forms the basis for this work. This model consists of approximate forms of the continuity and momentum equations for water of finite depth. The solution yields the surface elevation $\eta(\mathbf{x},t)$, where $\mathbf{x}=(x,y)$ is position in the horizontal plane, and the horizontal velocity $\mathbf{u}(\mathbf{x},t)=(u,v)$ at a reference depth $z=z_\alpha$. The reference depth is defined as $z_\alpha=\beta_0 h$ where $\beta_0=-0.531$ and $h=h(\mathbf{x})$ is the water depth.

2.1 Governing equations

For the work in this effort, the weakly nonlinear form of the model is used (after Wei *et al.*, 1996). It consists of a continuity equation

$$\eta_t = E(\eta,u,v)+\widetilde{S}(\mathbf{x},t)\ , \tag{1}$$

and two momentum equations

$$[U(u)]_t = F(\eta,u,v)+[F_1(v)]_t+F_s\ , \tag{2}$$

$$[V(v)]_t = G(\eta,u,v)+[G_1(u)]_t++G_s\ , \tag{3}$$

where

$$U = u + \left[b_1 h^2 u_{xx} + b_2 h \left(hu\right)_{xx}\right] , \tag{4}$$

$$V = v + \left[b_1 h^2 v_{yy} + b_2 h \left(hv\right)_{yy}\right] , \tag{5}$$

$$\begin{aligned} E = & -\left[\left(h+\eta\right) u\right]_x - \left[\left(h+\eta\right) v\right]_y \\ & - \left\{h\left[a_1 h^2 \left(u_{xx} + v_{xy}\right) + a_2 h \left(hu\right)_{xx} + a_2 h \left(hv\right)_{xy}\right]\right\}_x \\ & - \left\{h\left[a_1 h^2 \left(u_{xy} + v_{yy}\right) + a_2 h \left(hu\right)_{xy} + a_2 h \left(hv\right)_{yy}\right]\right\}_y , \end{aligned} \tag{6}$$

$$F = -g\eta_x - \left(uu_x + vu_y\right) , \tag{7}$$

$$G = -g\eta_y - \left(uv_x + vv_y\right) , \tag{8}$$

$$F_1 = -h\left[b_1 h v_{xy} + b_2 \left(hv\right)_{xy}\right] , \tag{9}$$

$$G_1 = -h\left[b_1 h u_{xy} + b_2 \left(hu\right)_{xy}\right] . \tag{10}$$

In addition, $\widetilde{S}(\mathbf{x}, t)$ in (1) is an internal 'wavemaker' source function, and F_s and G_s in (2) and (3), respectively, are source terms representing wave-breaking, bottom friction, etc.; these are discussed below. In the above expressions, $a_1 = \beta_0^2/2 - 1/6$, $a_2 = \beta_0 - 1/2$, $b_1 = \beta_0^2/2$ and $b_2 = \beta_0$; where $\beta_0 = z_\alpha/h = -0.531$.

The boundary conditions for these equations vary depending upon the situation. For a domain surrounded by an impermeable, perfectly reflecting boundary, the velocity and the surface-elevation gradient in the boundary-normal direction vanish at the boundary. Waves can be generated using a prescribed mass 'source' in a region which acts as a wavemaker. Alternatively, prescribed, time-varying values of velocity and surface elevation on the boundaries can account waves entering the domain from outside.

2.2 Additional physical models

The preceding equations apply to propagation of waves in a region of finite water depth, but do not adequately treat beaches, where the water depth goes to zero and the waves run up on the beach, or breaking waves where steep waves lose energy through dissipation while momentum is conserved. Additional models are necessary to capture these physical effects. In addition, to simulate real-world situations, a means for generating waves at the domain boundary is necessary. In this section,

wave run-up and wave-breaking models used in the Boussinesq model are described, along with the wave-generation approach used.

2.2.1 Wave run-up model

To accommodate wave run-up on a beach, a 'slot' run-up model is used. This model effectively allows the water surface to exist for the entire computational domain (including regions of dry beach). This is accomplished by relegating the water to narrow slots (or equivalently, porous regions) in the 'dry' portions of the domain. In the dry regions, the amount of water is kept negligibly small, but non-zero. As a wave crest approaches the beach, the slot rapidly fills and the water level rises above the bottom level; as the wave recedes, the water runs off until only the small amount that resides in the slot remains. The basic approach is described by Kennedy *et al.* (2000) and Chen *et al.* (2000); a slightly modified approach is used here.

The slot run-up method is implemented using a modified continuity equation, based on the exact equation (1), above. The modified equation is

$$\begin{aligned} \eta_t &= -\left\{A(\eta)u + h\left[a_1 h^2 \left(u_{xx} + v_{xy}\right) + a_2 h \left(hu\right)_{xx} + a_2 h \left(hv\right)_{xy}\right]\right\}_x \\ &\quad -\left\{A(\eta)v + h\left[a_1 h^2 \left(u_{xy} + v_{yy}\right) + a_2 h \left(hu\right)_{xy} + a_2 h \left(hv\right)_{yy}\right]\right\}_y + S(\mathbf{x},t)\ , \end{aligned} \tag{11}$$

where the run-up model is represented by $A(\eta)$. For no run-up modeling, $A(\eta) = h + \eta$; the model is invoked by setting

$$\begin{aligned} A(\eta) &= h_c + \eta && (h+\eta) \le 0 \\ &= (h+\eta) + (h_c - h)\ \delta && (h+\eta) > 0\ , \end{aligned} \tag{12}$$

where δ is the relative cross-sectional area of slots (δ is typically set to 0.02), and h_c is set to the maximum water depth in the domain.

This implementation of the slot run-up model undergoes an abrupt transition as the waves run up and 'fill' the slot, compared to the form of Kennedy *et al.* (2000), which has a gradual transition; however, in practice a gradual transition does not ensure smoothness in the horizontal derivatives of $A(\eta)$, and lack of smoothness can lead to instability. For this reason, a high-limit filter which

cuts off at twice the grid spacing is applied to $A(\eta)$, once it is calculated. This ensures well behaved derivatives and results in a robust model.

2.2.2 Wave breaking and bottom friction

Wave breaking is modeled in a manner similar to that described in Kennedy *et al.* (2000), i.e. by adding an additional diffusive term to the momentum equations. This is given by

$$F_{s,b} = \frac{1}{h+\eta}\left\{\nu_b\left[(h+\eta)u\right]_x\right\}_x + \frac{1}{2(h+\eta)}\left\{\nu_b\left[(h+\eta)u\right]_y + \nu_b\left[(h+\eta)v\right]_x\right\}_y \tag{13}$$

$$G_{s,b} = \frac{1}{h+\eta}\left\{\nu_b\left[(h+\eta)v\right]_y\right\}_y + \frac{1}{2(h+\eta)}\left\{\nu_b\left[(h+\eta)v\right]_x + \nu_b\left[(h+\eta)u\right]_y\right\}_x \tag{14}$$

where ν_b is the eddy viscosity associated with breaking. This eddy viscosity is defined after Zelt (1991) as

$$\nu_b = B\delta_b^2(h+\eta)\eta_t \tag{15}$$

where $\delta_b = 1.2$ and

$$B = \min\left[\max\left(0,\ \frac{\eta_t}{\eta_t^*} - 1\right),\ 1\right] . \tag{16}$$

where $\eta_t^* = 0.3\sqrt{g(h+\eta)}$. The form of (16) causes B to be bounded by zero and one and vary linearly between those limits as η_t increases from η_t^* to $2\eta_t^*$.

The effects of bottom friction are modeled via source terms in the momentum equations which oppose the fluid motion. The model form is given by

$$F_{s,f} = -C_b\frac{|\mathbf{u}|u}{h+\eta} \tag{17}$$

$$G_{s,f} = -C_b\frac{|\mathbf{u}|v}{h+\eta} , \tag{18}$$

where $C_b = 0.005$.

2.2.3 Wavemaker source function

Monochromatic waves are generated using a source term in the continuity equation (1), as described in Wei *et al.* (1999). The source function amplitude is set to

$$S_0 = \frac{\omega^2 - (\alpha_0 + \frac{1}{3})gk(kh_0)^3}{\omega\sigma k\left[1 - \alpha_0(kh_0)^2\right]} \; 2\eta_0 \; \cos(\theta) \tag{19}$$

where η_0 is the wave amplitude, ω is the wave circular frequency, θ is the wave direction measured counter-clockwise from the x axis, $k = 2\pi/\lambda$ is the wavenumber, h_0 is the fixed depth under the wavemaker, and $\alpha = b_1 + b_2$. Here, σ is given by

$$\sigma = \sqrt{\frac{\pi}{\beta_1}} e^{-k_x^2/4\beta_1} \tag{20}$$

where $k_x = k\cos(\theta)$ and $\beta_1 = 5(\lambda/2)^{-2}$. The source function used in (1) for a wavemaker located at $x = 0$ on the left-hand boundary of the computational domain is then given by

$$\begin{aligned} \widetilde{S}(\mathbf{x}, t) &= w(x)S(y, t) \\ &= e^{-\beta_1 x^2} \; S_0 \sin(k_y y - \omega t + \phi) \end{aligned} \tag{21}$$

where $w(x) = e^{-\beta_1 x^2}$, $k_y = k\sin(\theta)$ and $0 < \phi \leq 2\pi$ is an assigned phase.

For irregular waves, the spectral densities of the Fourier modes comprising the wave spectrum are converted to equivalent amplitudes and treated as monochromatic waves. The wavemaker source function is then given by

$$\widetilde{S}(\mathbf{x}, t) = \sum_{i}^{N_m} e^{-\beta_1 x^2} \; S_0^i \sin(k_y^i y - \omega^i t + \phi^i) \; , \tag{22}$$

where N_m is the number of modes and

$$S_0^i = \frac{(\omega^i)^2 - (\alpha_0 + \frac{1}{3})gk^i(k^i h_0)^3}{\omega^i \sigma^i k^i \left[1 - \alpha_0(k^i h_0)^2\right]} \; 2\eta_0^i \; \cos(\theta^i) \tag{23}$$

and

$$\sigma^i = \sqrt{\frac{\pi}{\beta_1}} e^{-(k_x^i)^2/4\beta_1} \ . \tag{24}$$

Here, the value of β_1 is calculated from the dominant wave (spectral peak), resulting in a fixed wavemaker width for all spectral components.

The present implementation allows the specification of the wave amplitude, period and direction from the command line for monochromatic waves. For irregular waves, a frequency–direction spectrum file in the FRF 8m Array format is read.

2.3 Numerical implementation

The Boussinesq equations incorporating the physical models described above are solved using a parallel FORTRAN code. The numerical implementation is identical to that described in Wei *et al.* (1996): explicit time integration using a third order predictor and an iterated fourth order corrector. The spatial grid is Cartesian with uniform spacing, and the grid is generated internally by the code. The solution is filtered every twenty time steps to eliminate spurious short-wavelength components (which result from numerical errors and nonlinearities and can accumulate due to the absence of natural diffusion or dissipation in the equations). The code is parallelized using domain decomposition and the message-passing interface (MPI). It will run for an arbitrary number of processors (the number of processors is specified on the command line) on both Linux (Portland Group compilers and LAM MPI) and SUN Microsystems (Forte compiler suite and MPICH MPI) platforms. Bathymetry information is read from a binary file on the same grid as the computational grid, while the tide is set via a command line argument.

3 The assimilation methodology

It is desired to determine the wavemaker source function which will yield predictions from the extended Boussinesq model which match most closely a set of time-series observations of the near-shore surface elevation and velocity. The approach taken will be based on the variational method described by Le Dimet & Talagrand (1986), corresponding to the 'strong-constraint' formalism

described by (Bennett, 1992, p. 148). The objective is to determine the source function which minimizes a 'cost function' (a positive-definite measure of the error in the predictions) subject to the constraint the the dynamical equations governing the wave field (the extended Boussinesq equations) are exactly satisfied.

The above constrained minimization problem is equivalent to the unconstrained minimization of the cost function 'augmented' with the product of the constraint equations and a set of 'adjoint' variables (i.e. Lagrange multipliers). The cost function will be minimized for the set of model inputs which correspond to a stationary point of this augmented cost function; i.e. where its first variation vanishes. The requirement that the first variation vanish yields the governing equations for the adjoint variables, as well as the relationship between the adjoint variables and the gradient of the cost function with respect to the control variables, i.e. the wavemaker source function.

In the following sections, the cost function and the augmented cost function are described. The first variation of the cost function is taken and the conditions under which the first variation vanishes, the Euler–Lagrange equations, are derived. The Euler–Lagrange equations are then used to develop both the adjoint equations and the relationship between the adjoint solution and the gradient of the cost function with respect to the wavemaker source function.

3.1 The cost function

The cost function is comprised of two parts. The first part is a measure of the error in the predicted wave field. The second part is based on the model input being estimated (i.e. the wavemaker source function), and is included to ensure a unique solution.

The first part of the cost function is a positive-definite measure of the error in the predicted wave field. Observations are taken to consist of time records of length T of the surface elevation and vector velocity at N discrete locations in the domain. In equation form, this is given by

$$J_1 = \sum_i^N \int_0^T \int_{\mathcal{R}} \left[\varphi_1 (\eta - \widehat{\eta}_i)^2 + \varphi_2 \frac{h_0}{g} (u - \widehat{u}_i)^2 + \varphi_3 \frac{h_0}{g} (v - \widehat{v}_i)^2 \right] \frac{\delta(\mathbf{x} - \mathbf{x}_i)}{NT} \, d\mathbf{x}dt \,, \quad (25)$$

where the circumflex indicates an observed quantity, the delta functions specify the locations of the observations, and the φ_k are constants which allow variable weighting of the different observation quantities. The integration here is over the entire space-time region of interest, $0 < t < T$ and for

all spatial locations $\mathbf{x} \in \mathcal{R}$.

The second part of the cost function is based on the estimated model inputs, in this case the wavemaker source function. In order to assure a unique solution, the input variable(s) must also be penalized via inclusion in the cost function (Bennett & Miller, 1991). This can be accomplished by including one or more positive-definite measures of the wavemaker source function, which leads to

$$J_2 = \int_0^T \int_{\mathcal{B}} \frac{h_0}{gL_sT} \left[\varphi_3 S^2(\xi,t) + \varphi_4 h_0^2 S_\xi^2(\xi,t) \right] d\xi dt \ , \tag{26}$$

where ξ indicates position along the centerline of the wavemaker $\mathcal{B}$ (which could correspond to a domain boundary), L_s is the length of the wavemaker, and S_ξ is the slope of the source function along the wavemaker. The first term constrains the source function to have minimum possible energy, while the second constrains the directional spread of the generated wave spectrum.

Combining J_1 and J_2 yields the complete cost function:

$$\begin{aligned} J = & \sum_i^N \int_0^T \int_{\mathcal{R}} \left[\varphi_1 \left(\eta - \widehat{\eta}_i \right)^2 + \varphi_2 \frac{h_0}{g} \left(u - \widehat{u}_i \right)^2 + \varphi_2 \frac{h_0}{g} \left(v - \widehat{v}_i \right)^2 \right] \frac{\delta(\mathbf{x} - \mathbf{x}_i)}{NT} \, d\mathbf{x} dt \\ & + \int_0^T \int_{\mathcal{B}} \frac{h_0}{gL_sT} \left[\varphi_3 S^2(\xi,t) + \varphi_4 h_0^2 S_\xi^2(\xi,t) \right] d\xi dt \end{aligned} \tag{27}$$

The methods of variational calculus (see e.g. Courant & Hilbert, 1953) show that minimizing the cost function J subject to the constraint that the solution satisfy the extended Boussinesq equations is equivalent to unconstrained minimization of an 'augmented' cost function. The physical solution variables are (η, u, v) and the corresponding governing equations are given by

$$\left(\{ \eta_t - E - wS \}, \{ U_t - F - F_{1t} \}, \{ V_t - G - G_{1t} \} \right) = 0. \tag{28}$$

(Here, the source terms in the momentum equations are ignored in the development of the adjoint equations.) A set of adjoint variables (α, β, γ) is introduced which correspond to (η, u, v). The cost function is augmented by the product of these adjoint variables and the governing equations (the

extended Boussinesq model). This augmented cost function $\mathcal{L}$ is given by

$$\mathcal{L} = J + \int_0^T \int_{\mathcal{R}} \Big[\alpha \{\eta_t - E - wS\} + \beta \{U_t - F - F_{1t}\} + \gamma \{V_t - G - G_{1t}\} \Big] d\mathbf{x}dt \, . \quad (29)$$

Here, $\mathcal{L}$ is a functional of α, β, γ, η, u, v and S, i.e. $\mathcal{L} = \mathcal{L}(\alpha, \beta, \gamma, \eta, u, v, S)$.

3.2 The Euler–Lagrange equations

The Euler–Lagrange equations define the conditions for the minimum of the augmented cost function. The cost function will be at a minimum for a stationary point, i.e. where the first variation of $\mathcal{L}$ the vanishes. The first variation is given by

$$\delta\mathcal{L} = \frac{\partial \mathcal{L}}{\partial \alpha} d\alpha + \frac{\partial \mathcal{L}}{\partial \beta} d\beta + \frac{\partial \mathcal{L}}{\partial \gamma} d\gamma + \frac{\partial \mathcal{L}}{\partial \eta} d\eta + \frac{\partial \mathcal{L}}{\partial u} du + \frac{\partial \mathcal{L}}{\partial v} dv + \frac{\partial \mathcal{L}}{\partial S} dS \quad (30)$$

and $\delta\mathcal{L} = 0$ for a stationary point. Hence, each of the terms in (30) must vanish independently, which requires that the partial derivatives of $\mathcal{L}$ all be zero: The resulting set of requirements that this imposes are the Euler–Lagrange equations. These are examined in the next sections.

3.2.1 The constraint equations

Setting the first three terms in (30) to zero yields the condition that the constraint equations, i.e. the extended Boussinesq model, must be satisfied at the minimum in $\mathcal{L}$. These terms are

$$\frac{\partial \mathcal{L}}{\partial \alpha} d\alpha = \int_0^T \int_{\mathcal{R}} [\{\eta_t - E - wS\} \, \delta\alpha] \, d\mathbf{x}dt \, , \quad (31)$$

$$\frac{\partial \mathcal{L}}{\partial \beta} d\beta = \int_0^T \int_{\mathcal{R}} [\{U_t - F - F_{1t}\} \, \delta\beta] \, d\mathbf{x}dt \, , \quad (32)$$

$$\frac{\partial \mathcal{L}}{\partial \gamma} d\gamma = \int_0^T \int_{\mathcal{R}} [\{V_t - G - G_{1t}\} \, \delta\gamma] \, d\mathbf{x}dt \, . \quad (33)$$

Since the regions for the integrations are arbitrary, the integrands must be identically zero for the integrals to vanish. In addition, the values of $\delta\alpha$, $\delta\beta$ and $\delta\gamma$ are arbitrary, the terms in braces must vanish independently. This requirement is the same as requiring the extended Boussinesq equations (1–3) to be satisfied exactly. (This is the 'strong' constraint on the wave field.) This essentially requires that the wave field which gives the minimum cost function (agrees best with

the observations) has the appropriate dynamics.

3.2.2 The adjoint Boussinesq equations

The next three terms of (30), those involving $\delta\eta$, δu and δv, yield a set of equations for the adjoint variables α, β and γ. The first variation of $\mathcal{L}$ with respect to η is given by

$$\frac{\partial \mathcal{L}}{\partial \eta} d\eta = \frac{\partial J}{\partial \eta} d\eta + \int_0^T \int_{\mathcal{R}} \left[\alpha \left\{ (\delta\eta)_t - \left(\frac{\partial E}{\partial \eta} \right) \delta\eta \right\} - \beta \left\{ \frac{\partial F}{\partial \eta} \right\} \delta\eta - \gamma \left\{ \frac{\partial G}{\partial \eta} \right\} \delta\eta \right] d\mathbf{x} dt \ . \tag{34}$$

Here, the U, V, F_1 and G_1 terms do not appear since they have no η dependence. After integrating by parts to move the $\delta\eta$s outside the derivatives and rearranging, the result is

$$\frac{\partial \mathcal{L}}{\partial \eta} d\eta = - \int_0^T \int_{\mathcal{R}} \left[\alpha_t - E' - \frac{2}{NT} \sum_i (\eta - \widehat{\eta}_i) \delta(\mathbf{x} - \mathbf{x}_i) \right] \delta\eta \ \ d\mathbf{x} dt \ , \tag{35}$$

where the final term in the brackets comes from the η-dependent term in the cost function. The first variation of (30) will vanish independent of the value of $\delta\eta$ only if the term in brackets is zero. This yields the governing equation for α, the adjoint of the variable η:

$$\alpha_t = E' + \frac{2}{NT} \sum_i (\eta - \widehat{\eta}_i) \delta(\mathbf{x} - \mathbf{x}_i) \ , \tag{36}$$

where

$$E' = -u\alpha_x - v\alpha_y - g(\beta_x + \gamma_y) \ . \tag{37}$$

To obtain the equation for β, the adjoint of u, we take the first variation with respect to u. This gives the result

$$\frac{\partial \mathcal{L}}{\partial u} du = \frac{\partial J}{\partial u} du + \int_0^T \int_{\mathcal{R}} \left[\alpha \left\{ -\frac{\partial E}{\partial u} \right\} \delta u + \beta \left\{ \frac{\partial U_t}{\partial u} - \frac{\partial F}{\partial u} - \right\} \delta u + \gamma \left\{ -\frac{\partial G}{\partial u} - \frac{\partial G_{1t}}{\partial u} \right\} \delta u \right] d\mathbf{x} \ dt \ . \tag{38}$$

After integrating by parts and collecting terms this yields

$$\frac{\partial \mathcal{L}}{\partial u} du = - \int_0^T \int_{\mathcal{R}} \left[\left[U'(\beta) \right]_t - F' - \left[F_1' \right]_t - \frac{2}{NT} \sum_i (u - \widehat{u}_i) \delta(\mathbf{x} - \mathbf{x}_i) \right] \delta u \ \ d\mathbf{x} \ dt \ . \tag{39}$$

The first variation of (30) will vanish independent of the value of δu only if the term in brackets is zero. This yields the governing equation for β, the adjoint of the variable u. The equation is

$$[U']_t = F' + [F_1']_t + \frac{2}{NT}\sum_i (u - \widehat{u}_i)\delta(\mathbf{x} - \mathbf{x}_i) \tag{40}$$

where

$$U' = \beta + \left[b_1(h^2\beta)_{xx} + b_2 h(h\beta)_{xx}\right] \tag{41}$$

$$\begin{aligned} F' = &-\left[(h+\eta)\alpha_x + a_1\left\{(h^3\alpha_x)_{xx} + (h^3\alpha_y)_{xy}\right\} + a_2 h\left\{(h^2\alpha_x)_{xx} + (h^2\alpha_y)_{xy}\right\}\right] \\ &+u_x\beta - (u\beta)_x - (v\beta)_y + v_x\gamma \end{aligned} \tag{42}$$

$$F_1' = -\left[b_1(h^2\gamma)_{xy} + b_2 h(h\gamma)_{xy}\right] . \tag{43}$$

The equation governing γ, the adjoint of v, can be derived by inspection from the β equation. Observing that the u and v equations are symmetric with respect to (u,v) and (x,y), i.e. interchanging x and y, as well as u and v, in the u equation (2) yields the v equation (3), and vice versa. A similar interchange in the η equation (1), yields (1). Hence, the governing equations for γ is

$$[V']_t = G' + [G_1']_t + \frac{2}{NT}\sum_i (v - \widehat{v}_i)\delta(\mathbf{x} - \mathbf{x}_i) \tag{44}$$

where

$$V' = \gamma + \left[b_1(h^2\gamma)_{yy} + b_2 h(h\gamma)_{yy}\right] \tag{45}$$

$$\begin{aligned} G' = &-\left[(h+\eta)\alpha_y + a_1\left\{(h^3\alpha_y)_{yy} + (h^3\alpha_x)_{xy}\right\} + a_2 h\left\{(h^2\alpha_y)_{yy} + (h^2\alpha_x)_{xy}\right\}\right] \\ &+v_y\gamma - (v\gamma)_y - (u\gamma)_x + u_y\beta \end{aligned} \tag{46}$$

$$G_1' = -\left[b_1(h^2\beta)_{xy} + b_2 h(h\beta)_{xy}\right] . \tag{47}$$

3.2.3 The cost function gradient

This final term in (30) involves the wavemaker source function $S(\xi, t)$, where ξ is the coordinate along the length of the wavemaker. (Here, $\mathbf{x} = (\zeta, \xi)$, where ξ is the coordinate along the wavemaker and ζ is the coordinate normal to the wavemaker; for the work presented here, $(\zeta, \xi) = (x, y)$, but

this is not general requirement.) If the constraint (Boussinesq) equations and the adjoint equations are satisfied, then last term in (30) is the only one that remains, and therefore

$$\delta\mathcal{L} = \frac{\partial \mathcal{L}}{\partial S} dS \ . \tag{48}$$

This quantity $\frac{\partial \mathcal{L}}{\partial S} dS$ contains contributions from the cost function and the continuity equation, where the wavemaker source S appears:

$$\begin{aligned} \delta\mathcal{L} &= \frac{\partial J}{\partial S} dS + \int_0^T \int_{\mathcal{R}} \Big[-\alpha \, w \delta S \Big] d\mathbf{x} \, dt \\ &= \int_0^T \int_{\mathcal{B}} \frac{2h_0}{gL_sT} \Big[\varphi_3 S \ \delta S + \varphi_4 h_0^2 S_\xi \ \delta S_\xi \Big] d\xi dt + \int_0^T \int_{\mathcal{R}} \Big[-\alpha \, w(\zeta) \ \delta S \Big] d\mathbf{x} \, dt \end{aligned} \tag{49}$$

Integrating by parts and collecting terms yields

$$\delta\mathcal{L} = \int_0^T \int_{\mathcal{B}} \left\{ \frac{2h_0}{gL_sT} \Big[\varphi_3 S - \varphi_4 h_0^2 S_{\xi\xi} \Big] - \int_{\mathcal{N}} \alpha(\zeta, \xi) \ w(\zeta) d\zeta \right\} \ \delta S \ d\xi dt \ , \tag{50}$$

where the integral inside the braces is over lines normal to the wavemaker centerline (indicated by $\mathcal{N}$), i.e. in the ζ-direction.

Equation (50) indicates that a small decrease in $\mathcal{L}$ (the thing we are trying to minimize) will result from a change in the source function δS given by

$$\delta S \propto - \left\{ \frac{2h_0}{gL_sT} \Big[\varphi_3 S - \varphi_4 h_0^2 S_{\xi\xi} \Big] - \int_{\mathcal{N}} \alpha(\zeta, \xi) \ w(\zeta) d\zeta \right\} \ . \tag{51}$$

Hence, the gradient of the augmented cost function $\mathcal{L}$ with respect to the wavemaker source function S is effectively given by

$$\frac{\partial \mathcal{L}}{\partial S} = \frac{2h_0}{gL_sT} \Big[\varphi_3 S - \varphi_4 h_0^2 S_{\xi\xi} \Big] - \int_{\mathcal{N}} \alpha(\zeta, \xi) \ w(\zeta) d\zeta \ . \tag{52}$$

This gradient can be used to determine the value of the wavemaker source function which will yield the best agreement between the estimated wave field and the observation data.

Examination of (52) shows that the gradient has three components. The first two depend on the source function S and its second derivative $S_{\xi\xi}$, and are included to produce a unique solution. The

third depends on the adjoint solution integrated over the region of the wavemaker. This portion of the gradient relates directly to the error in the predicted wave field .

3.3 Solution of the adjoint equations

The adjoint equations are similar in mathematical character to the extended Boussinesq equations (they also have identical linear dispersion properties). As a result, the same solution techniques that are used to solve the extended Boussinesq model equations can be applied to solve the adjoint equations. While the boundary and initial conditions for the adjoint equations are somewhat problem-dependent, a few general statements can be made.

The adjoint equations are solved for the time period for which the observations are available. They are integrated backward in time from the final time, $t = T$. The 'initial' conditions for the adjoint are $\alpha(\mathbf{x}, T) = \beta(\mathbf{x}, T) = \gamma(\mathbf{x}, T) = 0$.

The spatial boundary conditions for the adjoint equations are taken to be the same as for forward equations: α has zero-gradient conditions at all boundaries; $\beta = 0$ and $\gamma = 0$ a the x and y boundaries, respectively, and zero-gradient conditions elsewhere.

Each adjoint equation contains an 'observation' term for input of observations of the corresponding physical variable (η for the α equation, u for the β equations, and so on). Since the adjoint equations, and their boundary and initial conditions are otherwise homogenous, the observation terms are what make the adjoint solution non-zero. When the predictions for η, etc. agree exactly with the observations, the observation terms become zero, and the resulting solution to the adjoint equations is identically zero. The gradient of the cost function with respect to the inputs for the Boussinesq model will then be zero, and the assimilation procedure will have converged.

3.4 Assimilation algorithm

The cost function gradient calculated from the adjoint solution is used in a conjugate-gradient minimization scheme where cost function is minimized by adjusting the wavemaker source function. The procedure goes as follows:

1. The adjoint equations are solved backward in time with the observations as input and the gradient of the cost function with respect to the wavemaker source function is calculated from

the adjoint solution in the region of the wavemaker using (52).

2. The direction of steepest descent (opposite the gradient) is defined as the search direction.

3. The location of the minimum for the cost function along the search direction is determined using a secant method to find the location where the directional derivative (the inner product of the local gradient with the search direction) vanishes. Each iteration requires a forward model solution with the updated source function, and an adjoint model solution with the forward solution as input, followed by the calculation of the gradient from the adjoint solution.

4. The most recent gradient and the original search direction are used in the determination of the new search direction using the conjugate gradient scheme.

The last two steps represent a conjugate gradient cycle, and are repeated until the forward prediction converges. Once the procedure has converged, the most recent forward prediction represents the best fit to the observation data. The final wavemaker source function is saved to a file and can be used as input to the forward model to reproduce the best-fit wave prediction outside of the assimilation procedure.

This procedure is implemented in a parallel FORTRAN code which executes both the extended Boussinesq model and its adjoint and controls the conjugate gradient minimization algorithm. The code is parallelized using domain decomposition and the message-passing interface (MPI). As in the description of the Boussinesq model above, it will run for an arbitrary number of processors (the number of processors is specified on the command line) on both Linux (Portland Group compilers and LAM MPI) and SUN Microsystems (Forte compiler suite and MPICH MPI) platforms. Inputs are the same as for the Boussinesq model are described above with the addition of a data file for each of the data records used in the assimilation. Execution of the forward model or the assimilation procedure is controlled via command-line arguments, as are the parameters of the iteration scheme.

4 Forward Boussinesq model calculations

The extended Boussinesq model code including the wave-breaking and run-up models and the wavemaker source function was tested by calculating three different situations. The first was monochromatic waves propagating across a realistic bathymetry, derived from a survey for a 1 km

square area around the US Army Corps of Engineers Field Research Facility (FRF) in Duck, NC. This tested the basic wave propagation capabilities of the code and served as validation of the run-up model in particular (a run-up implementation that works on a planar beach is not necessarily robust enough for a realistic beach topography). The second case was the same bathymetry, but for irregular waves generated from a measured FRF wave spectrum. This tested the model for propagation and run-up of multiple wave modes, and also verified the broad spectrum directional wavemaker implementation.

4.1 Monochromatic waves

To test the basic wave generation, propagation and run-up in the Boussinesq model code, it was applied to a 1 km square region around the USACE FRF in Duck, NC. The model was run on a 2 m x 10 m (cross-shore by along-shore) grid. The bathymetry is shown in figure 1, and is seen to vary from zero to 8 m, with a bar located roughly 200 m offshore. There is a break in the bar at the location the FRF pier. To test the assimilation algorithm, synthetic measurements were extracted at the locations indicated in the figure, roughly at the crest of the bar.

The Boussinesq model was run for this bathymetry using a time step of 0.1 s. Waves were generated by a mass source at the left-hand boundary. The wavemaker source region centered at the boundary ($x = 0$), had a Gaussian profile and extended about 50 m into the computational domain. Waves were generated with a significant wave height $H_{mo} = 1$ m, a wave period of $T_p = 6$ s and by using a traveling wave (propagating in the $+y$-direction) in the source function were set to propagate at 10 degrees to the cross-shore direction. The resulting wave field is shown in figure 2. Here we can see that the waves run up on the beach and the water surface does not extend to the right-hand side of the domain. The wave field shown in the figure is a snapshot of the surface elevation after the waves have been running up on the beach several minutes of real time. For these calculations, wave absorbing layers are located within 50 m of the y boundaries to suppress reflections; this is responsible for the change in wave direction very near the boundaries.

In figure 2, seven locations spaced 100 m apart are indicated for which records of $\eta(t)$, $u(t)$ and $v(t)$ are saved. The velocity saved is for the reference depth z_α, about midway in the water column, although in shallow water the velocity is relatively uniform over depth. The temporal length of the records was several times the time required for a wave to traverse the computational domain,

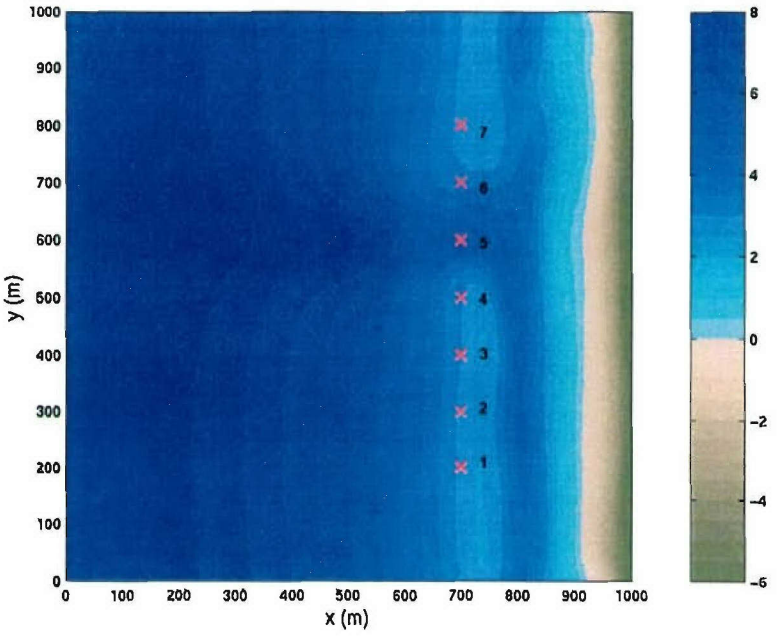

FIGURE 1. Bathymetry used in simulations for a 1 km square area around the USACE Field Research Facility at Duck NC.

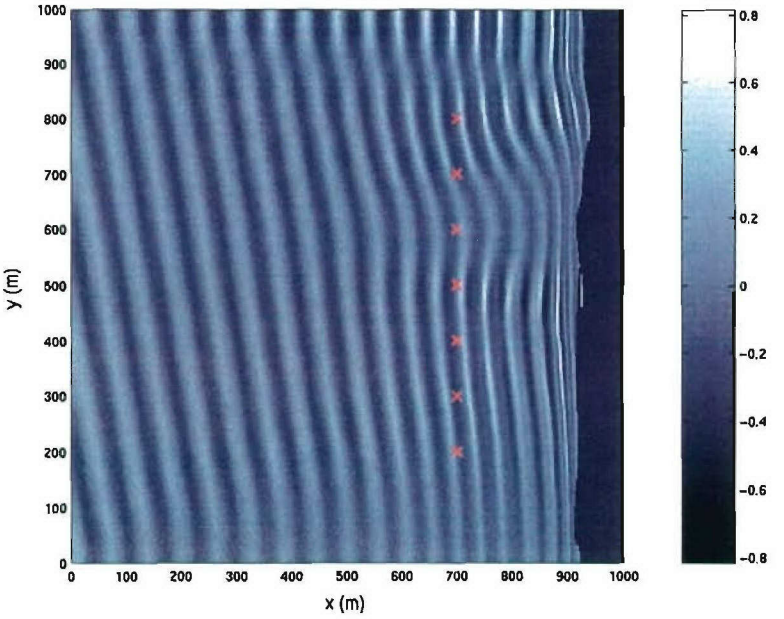

FIGURE 2. Monochromatic waves with $H_{mo} = 1\ m$, $T_p = 6\ s$ propagating at 10 degrees to the cross-shore direction over the bathymetry of figure 1, above. The waves are generated at the left, offshore boundary and run up on the beach at the right.

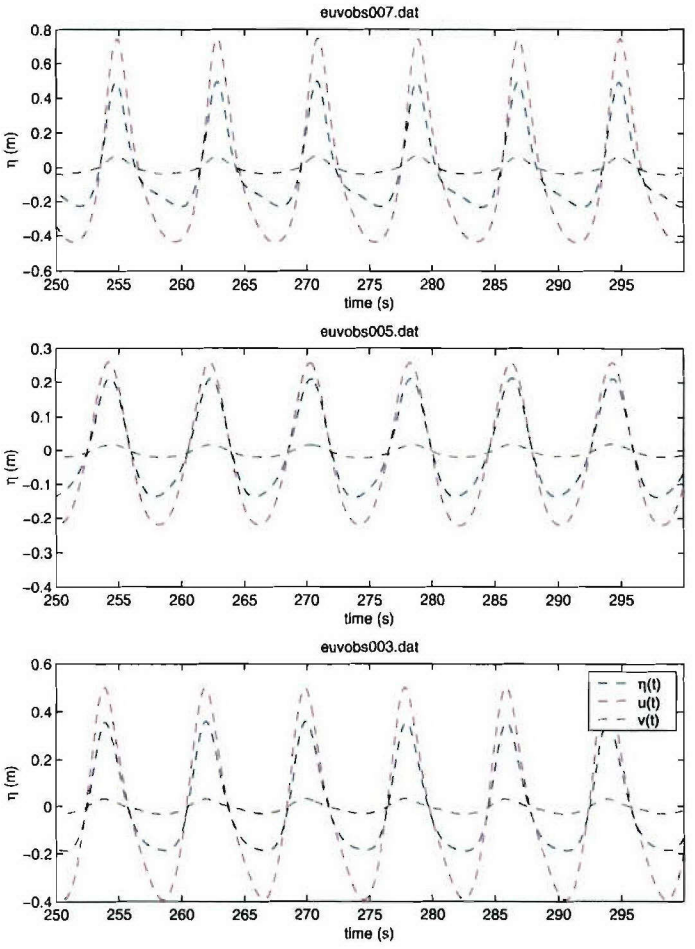

FIGURE 3. Sample wave records showing $\eta(t)$, $u(t)$ and $v(t)$ for locations 3, 5 and 7 in figure 1, above.

and the sampling rate was 0.1 sec, the computational time step. A portion of three of those time records is shown in figure 3.

4.2 Irregular waves

To calculate realistic wave fields using the extended Boussinesq model code, broad-spectrum waves must be generated. A broad-spectrum wavemaker, described above in section 2.2.3 was implemented. This wavemaker takes as input a spectrum in the format of the FRF 8m array, ASCII output file. Figure 4 shows a snapshot of the wave field generated using a measured FRF spectrum as input. The wave field has a significant wave height of 1.3 m, a peak wave period of 5.5 s and

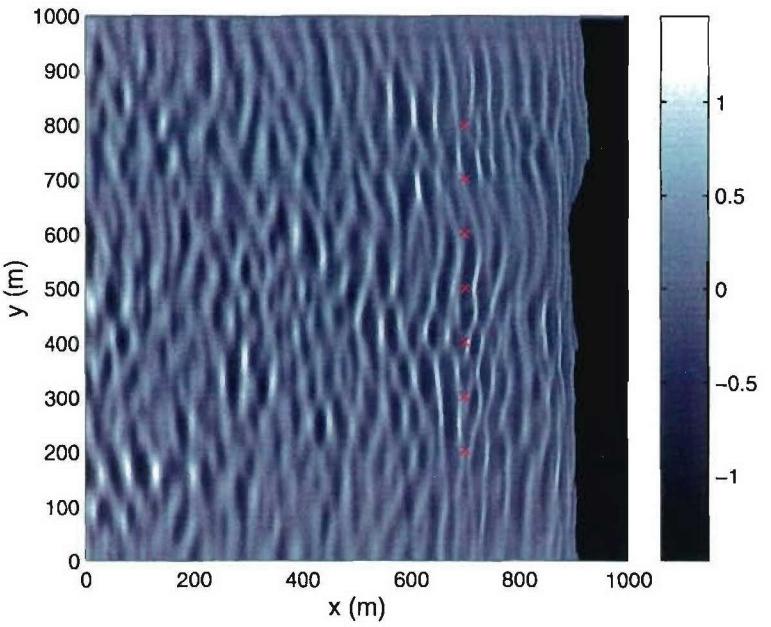

FIGURE 4. Irregular waves with $H_{mo} = 1.3\ m$, $T_p = 5.5\ s$ with a dominant wave direction roughly cross-shore propagating over the bathymetry of figure 1, above. The waves are generated at the left, offshore boundary and run up on the beach at the right.

the dominant wave direction is in the cross-shore direction. Figure 5 shows a 30-minute average of the surface elevation and velocity for the wave field shown in figure 4. Time histories of η, u and v from locations 2, 4 and 6 in figure 1 are shown in figure 6.

Broad-spectrum waves represent a challenge for nonlinear Boussinesq models. The long waves with higher propagation speeds set the requirements for the time step (based on the local Courant number). The short waves set the spatial grid requirements. In addition, the presence of multiple Fourier components and the nonlinearity of the model leads to the generation of sum and difference frequencies. These can lead to accumulation of spurious wave energy in wavelengths near the grid spacing (sawtooth waves). The results shown in figure 4, which represents the wave field at the end of 30 minutes of real-time evolution, shows no evidence of any short-wave noise.

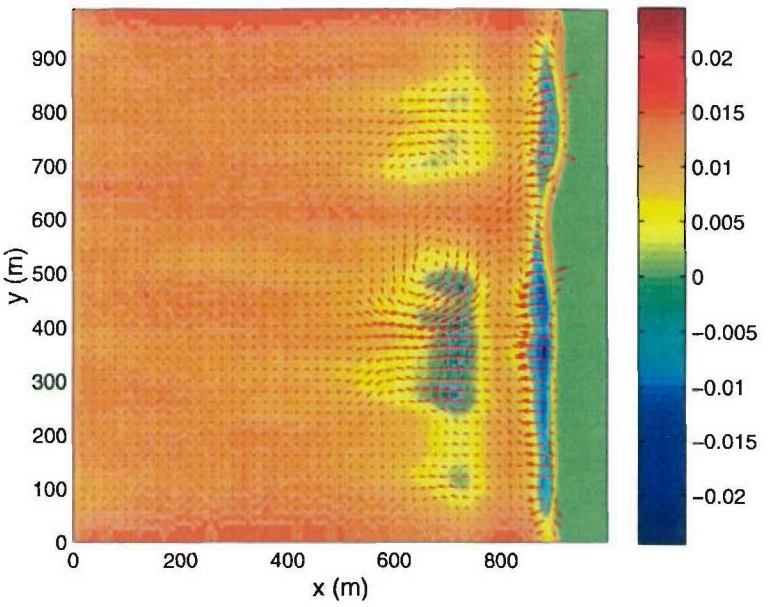

FIGURE 5. Results from Boussinesq calculations of irregular waves for a 30 min period: mean wave height overlaid with mean velocity vectors (the maximum mean velocity is 0.35 m/s) .

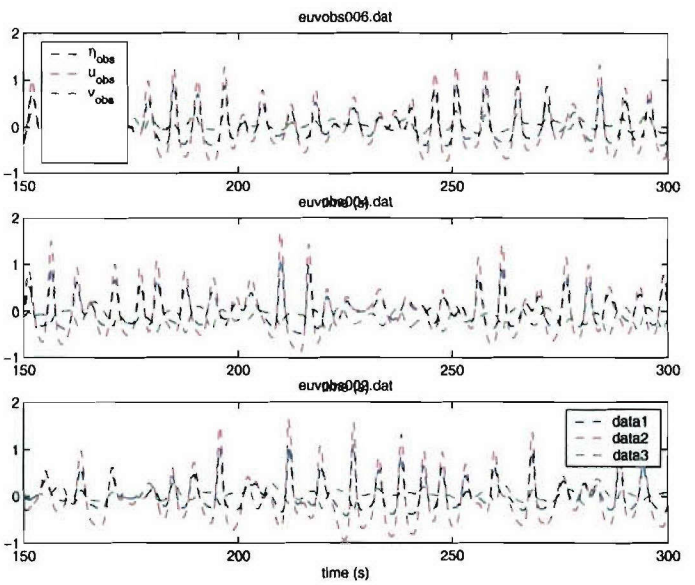

FIGURE 6. Time records of $\eta(t)$, $u(t)$ and $v(t)$ for locations 2, 4 and 6 in figure 1.

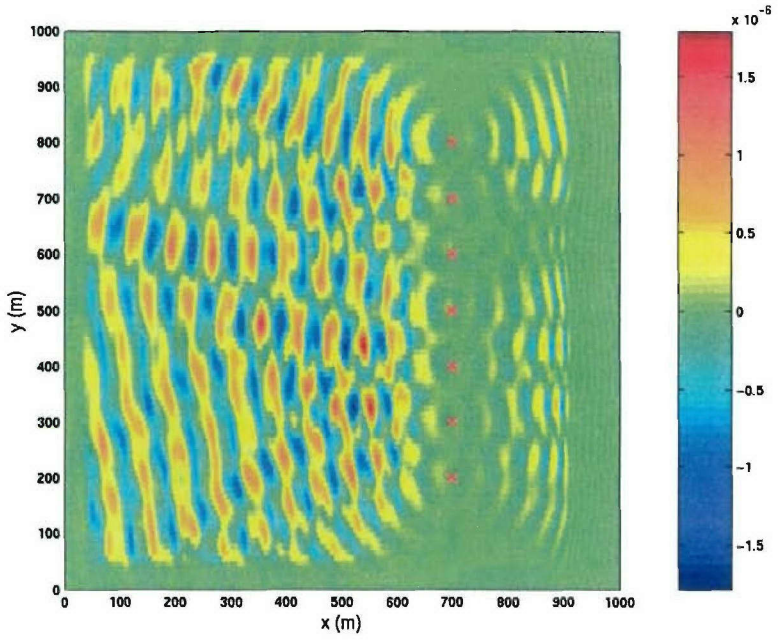

FIGURE 7. The adjoint solution $\alpha(\mathbf{x}, t)$ for the seven in-situ observations of the monochromatic wave field. The gradient of the cost function with respect the wave maker source function is calculated from the adjoint solution near the left boundary.

5 Assimilation results

In this section, the assimilation algorithm is applied using observations generated using both the monochromatic and irregular wave simulations described above.

5.1 Results for monochromatic waves

Time records of surface elevation and velocity for monochromatic waves were assimilated into the Boussinesq model using the procedure outlined above. This was done for the wave field shown above in section 4.1. The first step in the procedure is to solve the adjoint Boussinesq equations using the observations as input. A snapshot of the resulting adjoint solution is shown in figure 7. This figure shows the adjoint surface elevation field $\alpha(\mathbf{x})$. The adjoint solution near the left-hand boundary is used to calculate the gradient of the cost function with respect to the wavemaker source function.

Figure 8 shows the iteration history of the cost function. The complete cost function J_{Total}

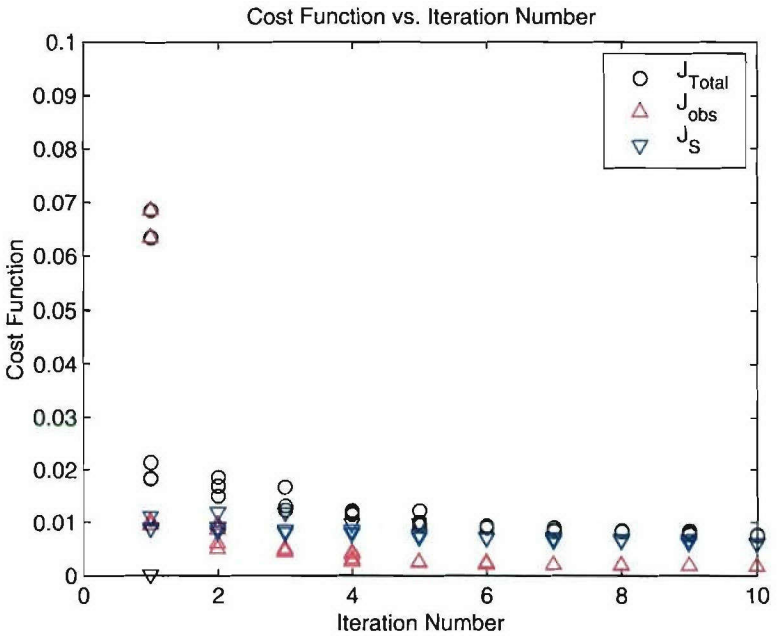

FIGURE 8. Iteration history of the cost function J_{Total} (27) for monochromatic waves along with the contributions from the observations J_{obs} (25) and the source function J_s (26); here each iteration corresponds to a conjugate-gradient cycle. This results shows that the cost function is reduced substantially and converges in less that ten iterations.

defiend by (27), above, is shown, along with the components attributed to the observations J_{obs} (25) and that attributed to the wavemaker source function J_s (26). Each 'iteration' in the figure shows the multiple values that are obtained during a conjugate-gradient cycle. As the iterations proceed, the portion of the cost function attributed to the observations decreases, while that from the source function increases, as is expected. The overall cost function J decreases and levels out after about 5 iterations, and is clearly converged by ten iterations.

The estimated sea surface resulting from the assimilation procedure is shown in figure 9. With the exception of some small undulations in the wave crests, the wave field is reproduced with good accuracy. Figure 10 shows a comparison between the time-series observations used in the assimilation process and those from the resulting estimate. Again the agreement is quite good.

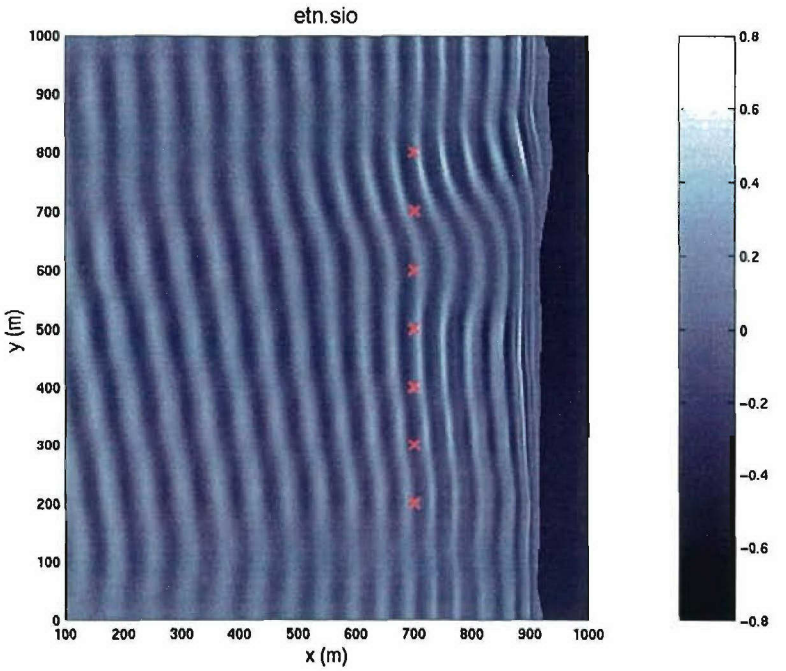

FIGURE 9. Sea surface elevation estimated using the assimilation procedure; this result compares well to the actual sea surface shown in figure 2.

5.2 Results for irregular waves

Time records of surface elevation for the irregular waves of section 4.2 were assimilated into the Boussinesq model using the procedure outlined above. The iteration history of the cost function is shown in figure 11. Here it can be seen that the cost function reduction is less than for the monochromatic waves, shown above, and there is only about a factor of two reduction.

A snapshot the estimated wave field is shown in figure 12, compared to the corresponding snapshot from the actual wave field. Comparison of the two images shows that while the long-wave components of the sea surface are captured well, the short-wave components are missing from the estimated sea surface. This is particularly true of short-wave components propagating in the alongshore direction. Figure 13 shows a comparison between the time-series observations used in the assimilation process and those from the resulting estimate. Overall the lower frequency component are captured, but the higher frequency components, in particular in the v velocity are missed. The level of error in the u velocity estimate is comparable to that in the v velocity indicating that oblique waves are not being well captured.

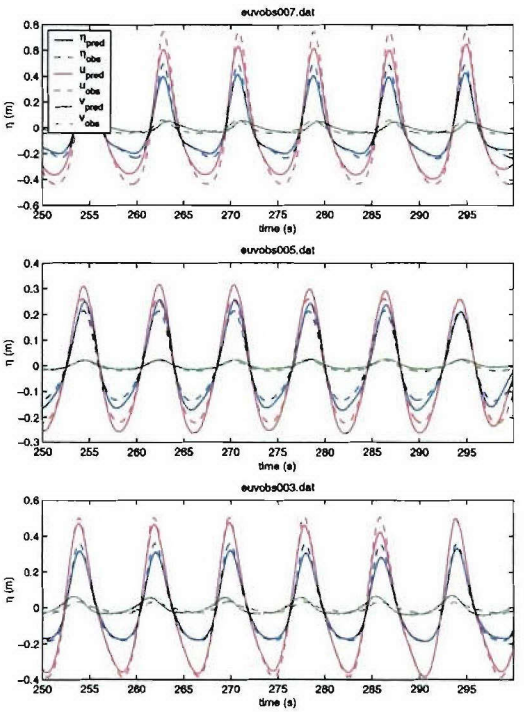

FIGURE 10. Comparison of estimated and actual time histories at the observation locations.

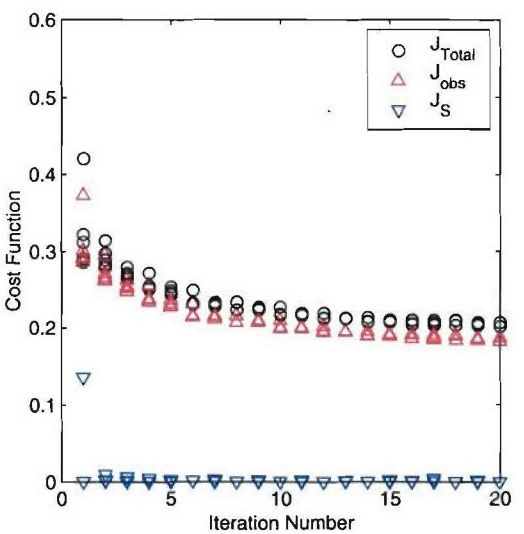

FIGURE 11. Iteration history for the cost function J_{Total} (27) along with the contributions from the observations J_{obs} (25) and the source function J_s (26); here each iteration corresponds to a conjugate-gradient cycle.

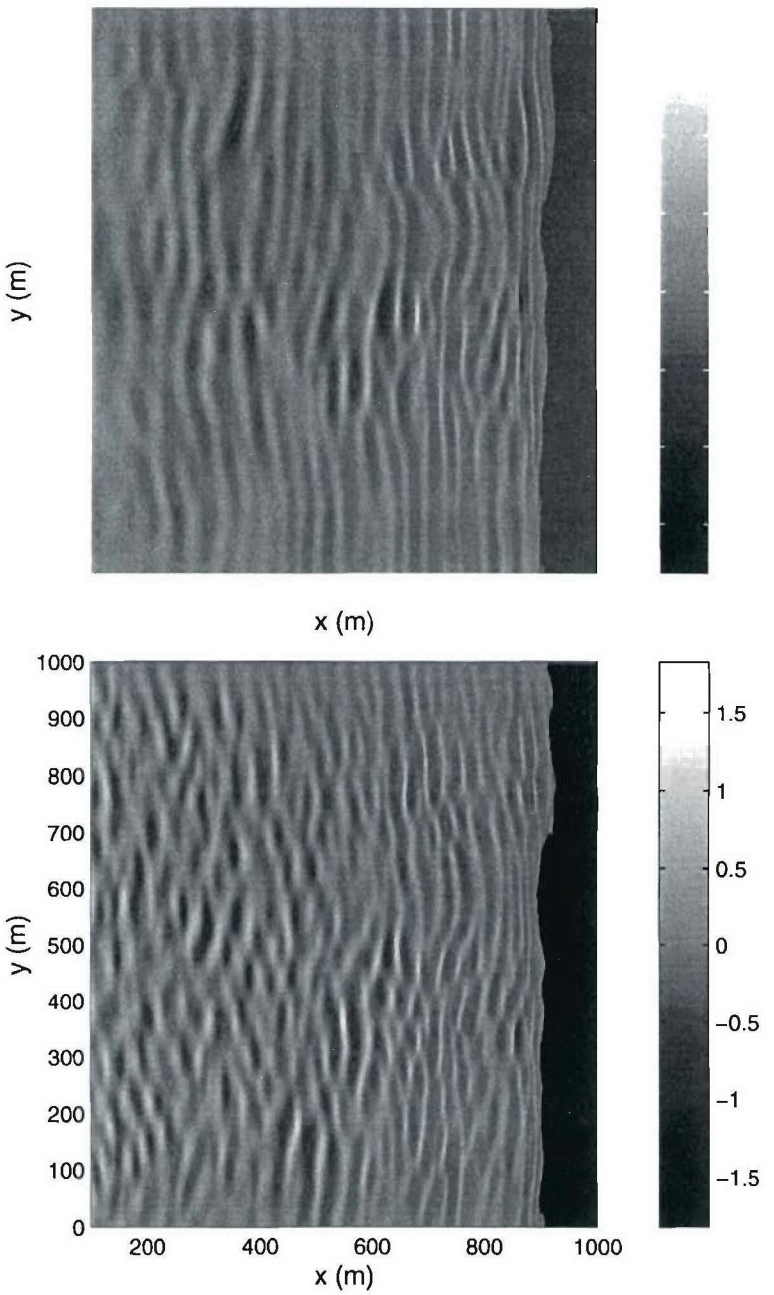

FIGURE 12. a) Sea surface elevation estimated using the assimilation procedure. b) Actual sea surface corresponding to the time for the estimated sea surface. The estimated wave field captures the longer wavelength components of actual sea surface.

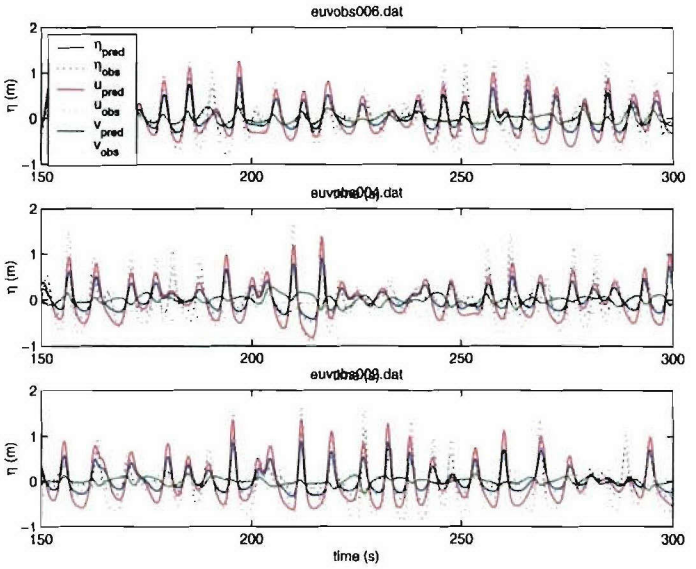

FIGURE 13. Comparison of estimated and actual time histories at the observation locations.

6 Conclusions and recommendations

This report describes a variational approach for assimilation of single-point in-situ observation of surface elevation and velocity into the extended Boussinesq model of Wei *et al.* (1996). The mathematical framework for assimilation is presented, along with applications of the procedure for two cases: monochromatic waves and broad-spectrum irregular waves. Overall the performance of the approach for monochromatic waves is quite good; while for irregular waves, some of the short-wave detail, especially for waves propagating in the along-shore direction, is missed. As part of the development work for the assimilation procedure a parallel Boussinesq model code was improved through addition of run-up, wave-breaking and and bottom-friction models, and a directional wavemaker was implemented.

The assimilation methodology is based on a variational approach wherein the wavemaker source function for the Boussinesq model which results in a best fit between the calculated wave field and the observations is determined. To do this, a cost function is defined which is a positive-definite measure of the error between the predictions and observations. The control variable, that which is adjusted to produce the desired wave field, is the wavemaker source function for the Boussinesq model. To find the minimum in the cost function, subject to the constraint that the

estimated wave field satisfy the extended Boussinesq equations, the cost function is augmented with the Boussinesq equations weighted with the adjoint variables. Setting the first variation of the augmented cost function with respect to the solution variables and the adjoint variables results in the conditions required for a minimum; it also produces the adjoint equations. The solution of the adjoint equations is used to calculate the gradient of the cost function with respect to the control variable. This gradient is used in a conjugate-gradient iteration scheme to find the wavemaker source function which yields the best fit to the data as measured by the cost function. Additional terms related to the wavemaker source function are included in the cost function to ensure a unique result.

As part of the code development for this effort, and existing parallel Boussinesq code based on both the formulation and numerical approach of Wei *et al.* (1996), was extended to include modeling for run-up, wave-breaking and bottom friction. In addition both monochromatic and broad-spectrum wavemakers were implemented. This results in a Boussinesq model code capable of generating realistic wave fields either as a product of the assimilation process, or as a direct forward prediction based on a known incident wave spectrum.

The assimilation procedure was applied to two cases, observations of monochromatic waves and irregular waves. Application of the procedure for monochromatic waves results in a converged solution after about five conjugate gradient iteration cycles. Comparison of the spatial variations in the wave field at an instant in time reveals some spatial undulations in the estimated wave field, but otherwise good agreement. This indicates that some spurious higher-wave-number components have been introduced by the assimilation procedure. Comparison of the estimated time series at the observation locations to the observations shows good agreement between the predictions and observations.

Use of the assimilation procedure for data derived from broad-spectrum irregular waves produces encouraging, but less-good results. The assimilation procedure converges in about ten iterations, although it continues to drop, albeit slowly, for about ten more iterations. The results estimate of the wave field reproduces the longer wavelength components, while shorter wavelength components are missed. This is especially true for the along-shore propagating wave components.

The approach developed and presented here appears promising, allowing the entire wave field to be estimated from a set of single-point in-situ observations. The resulting estimate is consistent

with the physics of near-shore waves as represented in extended Boussinesq models. The work under this effort is, however, primarily a demonstration that such an approach to the problem is feasible. Additional necessary work includes:

- Exercising the assimilation algorithm for a broad range of simulated wave fields to determine the limitations of the resulting wave estimates.
- Application of the assimilation algorithm to field observation and comparison to other ground-truth data.
- Investigation of alternative approaches to ensuring uniqueness of the resulting wave field. The present approach penalizes spatial gradients in the wavemaker source function and may result in suppression of along-shore waves; and an alternative approach which does not have this effect would be desirable.

Finally, the assimilation algorithm described here allows one to relate a set of single-point in-situ observations to a synoptic picture of the wave field. This ability can most likely be exploited to develop methods to determine an optimal approach for observing waves in a give region, i.e. an approach which extracts the maximum amount of information from the minimum number of observations.

References

BENNETT, A. F. 1992 *Inverse Methods in Physical Oceanography*. Cambridge.

BENNETT, A. F. & MILLER, R. N. 1991 Weighting initial conditions in variational assimilation schemes. *Monthly Weather Rev.* **119**, 1098.

CHEN, Q., KIRBY, J. T., DALRYMPLE, R. A., KENNEDY, A. B. & CHAWLA, A. 2000 Boussinesq modeling of wave transformation, breaking and runup. II: 2D. *J. Wtrwy, Port, Coast. and Oc. Engrg* **126**, 48–56.

COURANT, R. & HILBERT, D. 1953 *Methods of Mathematical Physics*. Wiley Interscience.

KENNEDY, A. B., CHEN, Q., KIRBY, J. T. & DALRYMPLE, R. A. 2000 Boussinesq modeling of wave transformation, breaking and runup. I: 1D. *J. Wtrwy, Port, Coast. and Oc. Engrg* **126**, 39–47.

LE DIMET, F.-X. & TALAGRAND, O. 1986 Variational algorithms for analysis and assimilation of meteorological observations: theoretical aspects. *Tellus* **38***A*, 97–110.

WEI, G., KIRBY, J. T., GRILLI, S. T. & SUBRAMANYA, R. 1996 A fully nonlinear Boussinesq model for surface waves. Part 1. Highly nonlinear unsteady waves. *J. Fluid Mech.* **294**, 71–92.

WEI, G., KIRBY, J. T. & SINHA, A. 1999 Generation of waves in boussinesq models using a source function method. *Coastal Engineering* **36**, 271–299.

ZELT, J. A. 1991 The run-up of nonbreaking and breaking solitary waves. *Coast. Engrg* **15**, 205–246.